Molecular dynamics simulation of a solid platinum nanowire under uniaxial tensile strain: Temperature and strain-rate effects

S. J. A. Koh, H. P. Lee, C. Lu, and Q. H. Cheng
Institute of High Performance Computing, 1 Science Park Road, #01-01, The Capricorn, Singapore Science Park II, Singapore 117528, Singapore

(Received 18 January 2005; revised manuscript received 13 April 2005; published 3 August 2005)

Nanoscale research has been an area of active research over the past fifteen years. This is due to the overall enhanced properties of nanomaterials due to size effects, surface effects, and interface effects, which typically showed up in materials with characteristic size smaller than 100 nm. This study focuses on the molecular dynamics (MD) simulation of an infinitely long, cylindrical platinum nanowire, with an approximate diameter of 1.4 nm. The nanowire was subjected to uniaxial tensile strain along the [001] axis. The changes in crystal structure during deformation were analyzed and its mechanical properties were deduced from the simulation. Classical MD simulation was employed in this study, with the empirical Sutton-Chen pair functional used to describe the interatomic potential between the platinum atoms. The Berendsen loose-coupling thermostat was selected for finite-temperature control of the simulated system, with a time constant of 25% of the total relaxation time during each strain increment. The nanowire was subjected to strain rates of 0.04%, 0.4%, and 4.0% ps^{-1}, at simulation temperatures of 50 and 300 K, in order to study the effects of different strain rates and thermal conditions on the deformation characteristics and mechanical properties of the nanowire. It was found that the stress-strain response of the nanowire showed clear periodic, stepwise dislocation-relaxation-recrystallization behavior at low temperature and strain rate, where crystal order and stability were highly preserved. The onset of amorphous crystal deformation occurred at 0.4% ps^{-1}, and fully amorphous deformation took place at 4.0% ps^{-1}, with amorphous melting detected at 300 K. Due to higher entropy of the nanowire at higher temperature and strain rate, periodic stress-strain behavior became less clearly defined, and superplasticity behavior was observed. This characteristic was significantly enhanced due to the development of a single-walled helical substructure at 300 K, when the nanowire was deformed at a lower strain rate. The Young's modulus was found to be about 50% to 75% that of its bulk counterpart, while the Poisson ratio was not significantly changed at the nanoscale.

DOI: 10.1103/PhysRevB.72.085414 PACS number(s): 68.65.−k, 62.25.+g, 62.20.−x, 02.70.Ns

I. INTRODUCTION

Nanostructures like nanotubes, nanowires, nanobelts, and nanoclusters have extraordinary mechanical, electrical, thermal, and magnetic properties. Nanoresearch has flourished over the past decade as a result of promising applications due to the overall enhanced properties at the nanoscale.[1] In particular, metallic nanowires have several useful applications, which were identified in nanoscale wiring of integrated circuits,[2] nanowire arrays for opto-electronic applications,[3] and usage as tips for scanning tunneling microscope (STM) and atomic force microscope (AFM).[4] Nanowires were also employed for catalysis, as a superconductor,[5] and as nanopipette probes.[6]

Numerous studies had been dedicated to fabrication, experimentation, and simulation of metallic nanowires,[7–10] among which, much work has been done for the simulation of gold nanowires. A couple of studies were dedicated to ascertaining the properties of gold nanowires in the nanoscale regime.[11–14] Recently, Zhang *et al.*[15] investigated the structure and properties of nickel nanowires. Ercolessi *et al.* used the glue model[16]—a modified form of the embedded atom model proposed by Daw and Baskes[17]—for molecular dynamics (MD) simulation of gold surfaces. Ju *et al.*[18] simulated the tensile behavior of ultrathin, single-shell nanowires; Bilalbegović[19] performed MD simulation on a multishell gold nanowire structure and studied its behavior under uniaxial compression. Pokropivny *et al.*[20] studied the *in situ* transformations of nanoscale gold contacts using MD simulation, and its results were also verified experimentally in the same study. Kang and Hwang[21] investigated the size and strain-rate effects on the axial elongation and horizontal shear behavior of copper nanowires. At low strain rates of 0.002% and 0.02% ps^{-1}, it was found that the higher stretch velocity caused the first yield strain to decrease, the period of yielding and recrystallization to be shortened, and both the rupture strain and the magnitude of force relaxation to be reduced. On the other hand, Ikeda *et al.*[22] and Braníco and Rino[23] simulated nickel and NiCu nanowires at extremely high strain rates of up to 15% ps^{-1}, which revealed strain hardening and amorphization of the original face-centered cubic (fcc) crystal structure.

Platinum nanowires recently found applications in molecular electronics,[24] nanoactuators,[25] and very-high-frequency (VHF) nanoelectromechanical systems (NEMSs).[26] Such applications require the nanowires to be strained and relaxed at extremely high velocities and displacement amplitudes. Although many studies have been focused on gold, copper, and nickel nanowires, very few studies have been dedicated to the study of platinum nanowires.[27,28] The effects temperature and strain rate have on the mechanical properties of platinum nanowires have not been reported.

 ©2005 The American Physical Society

This paper presents a MD simulation performed on a cylindrical, solid platinum nanowire (NW) with a diameter of approximately 1.4 nm. The nanowire was subjected to uniaxial tensile strain, with simulation performed at temperatures of 50 and 300 K. The former corresponds to the melting point regions of atmospheric gases like O_2 (54.8 K) and N_2 (63.1 K), and the latter is the laboratory room temperature. At each simulation temperature, the NW is subjected to strain rates of 0.04%, 0.4%, and 4.0% ps^{-1}. This is equivalent to approximate stretch velocities of 1.2, 11.8, and 117.6 m/s for a 3.0-nm-long nanowire whisker, respectively. The lowest velocity typically occurs in the drawing of a whisker of metallic atoms by STM or AFM from the surface of a substrate.[4,29] Some interesting work was done by Todorov and Sutton[30] and Mehrez and Ciraci[31,32] in simulating the mechanical tensile behavior of connective gold and copper necks, respectively, which were formed between a sample substrate and a metal tip. Exceptionally large yield strengths were observed for the nanowires and quantum conductance jumps within the nanowire were found to correspond to abrupt atomic lattice rearrangements. The moderately fast velocity could be inherent in nanoactuators,[25] during sensing of moderate to high-pressure conditions, and the rapid stretch velocity would probably be observed in VHF NEMSs,[26] which is about 35% of the supersonic velocity. This study analyzes the temperature and strain-rate effects on the first yield stress and strain, relaxation characteristics, slip behavior, deformation characteristics of the crystal structure during strain, Young's modulus, and Poisson ratio of a platinum nanowire.

II. SIMULATION METHODOLOGY

MD simulation was performed on a solid fcc platinum nanowire with an approximately circular cross section of diameter 1.4 nm. An infinitely long platinum nanowire was modeled by the application of periodic boundary conditions in the [001] direction only. The other two Cartesian directions ([100] and [010]) were modeled with vanishing boundary conditions (that is, the planes orthogonal to these axial directions correspond to free surfaces). Following the model simulated by Finbow *et al.*,[27] 15 atomic layers were modeled within the simulation cell, giving a 360-atom platinum nanowire for this study. Figure 1 shows the platinum nanowire at its initial, underformed state.

The behavior of the nanowire under uniaxial strain was simulated using classical MD.[33] The validity of the classical MD approximation was verified by comparing the nearest-neighbor separation of 2.77 Å for platinum, to its de Broglie thermal wavelength, which was computed to be 0.0721 Å.[34] This makes quantum disturbances to the system negligible and hence the comparatively more time-consuming *ab initio* simulation does not offer significantly better accuracy of results as compared to classical MD.[35] While pairwise additive potentials were typically employed for classical MD simulation of fluids and rare gases,[36] they fail badly for the modeling of solids with many-body effects, especially for transitional metals and semiconductors.[37] In this simulation, the pair functional form was selected for the interatomic potential energy,[38] as follows:

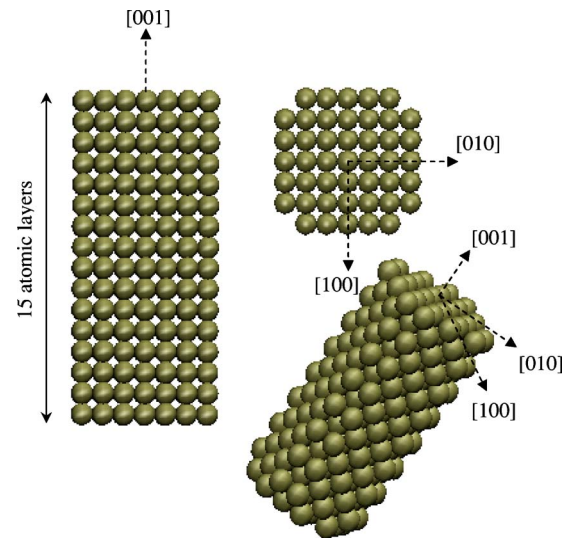

FIG. 1. (Color online) 360-atom platinum nanowire at its initial state.

$$V = \frac{1}{2}\sum_{\substack{i,j=1\\(j\neq i)}}^{N} \phi(r_{ij}) + \sum_{i=1}^{N} U(s_i) \tag{1}$$

where s_i is the pair function describing the local environment of atom i, relative to the contributions from its neighbors. $U(s_i)$ is the energy function, which relates the pair function to the local energetic environment. $\phi(r_{ij})$ is the conventional pairwise additive potential term.

Finnis and Sinclair[39] used the second-moment approximation of the tight-binding formulation[40] to derive a nonlinear energy function, as follows:

$$U(s_i) = \sqrt{s_i} \tag{2a}$$

and

$$s_i = \sum_{\substack{j=1\\(j\neq i)}}^{N} \rho(r_{ij}). \tag{2b}$$

Cleri and Rosato[41] showed that the empirical potential described above has the capability of describing fcc and hcp transition metals in a realistic manner. It was verified by calculating point-defect properties, lattice dynamics, and finite-temperature behavior, and comparing them to experimental results and other potential schemes. Sutton and Chen[42] parametrized the potential function given in Eqs. (1) and (2) for fcc metals, the following form was used:

$$E_{SC} = \varepsilon\left[\frac{1}{2}\sum_{i=1}^{N}\sum_{\substack{j=1\\(j\neq i)}}^{N} \phi(r_{ij}) - c\sum_{i=1}^{N}\sqrt{s_i}\right] \tag{3a}$$

and

TABLE I. Optimized parameters of pair functional for platinum.

Functional parameter	Optimized value
a (Å)	3.92
ε (meV)	19.833
c	34.408
m	8
n	10

$$\phi(r_{ij}) = \left(\frac{a}{r_{ij}}\right)^n, \quad s_i = \sum_{\substack{j=1 \\ (j\neq i)}}^{N} \left(\frac{a}{r_{ij}}\right)^m. \tag{3b}$$

Equation (3) consists of a pairwise additive potential that models the repulsive energy, and the N-body pair functional gives the cohesive energy. The constant a in Eq. (3b) is fixed to the crystal lattice parameter, and ε, c, m, and n are optimized against the equilibrium crystal configuration, cohesive energy per atom, bulk modulus, and elastic constants C_{11}, C_{12}, and C_{44}. Table I shows the optimized parameters for platinum.

Differentiating Eq. (3) with respect to r_{ij}, the total force of the system is

$$\mathbf{F}_{SC} = -\frac{\varepsilon}{r_{ij}} \sum_{j\neq i} \left[n\left(\frac{a}{r_{ij}}\right)^n - \frac{mc}{2}(s_i^{-1/2} + s_j^{-1/2})\left(\frac{a}{r_{ij}}\right)^m \right] \hat{\mathbf{r}}_{ij}, \tag{4}$$

where $\hat{\mathbf{r}}_{ij}$ is the unit vector of $\mathbf{r}_{ij}$, the interatomic vectoral expression between atoms i and j.

The atomic positions, velocities, and intermolecular forces for each time step are obtained by solving Newton equations of motions, using the velocity-Verlet numerical integration scheme.[33,34] The atomic velocities were scaled against the simulation temperature using the Berendsen thermostat.[43] The simulated strain rate is given as

$$\dot{\varepsilon}_{zz} = \frac{\Delta\varepsilon_{zz}}{S\Delta t}, \tag{5}$$

where $\varepsilon_{zz}=\Delta L_z/L_z$ is the nominal strain of the nanowire at each time step [this is not to be confused with the energy parameter (ε) in Eqs. (3) and (4)]. $\Delta\varepsilon$ is therefore the strain increment, which has been fixed at 0.4% strain per increment. S is the number of relaxation steps after each strain increment and Δt is the simulation time step. In this simulation, the number of relaxation steps was fixed at 10 000 steps, while the time step was varied, using $\Delta t=1.0$, 0.1, and 0.01 fs, simulating strain rates of 0.04%, 0.4%, and 4.0% ps^{-1}, respectively. During the simulation, atomic velocities were rescaled four times over the relaxation period, resulting in a coupling constant of $\tau=2.5$, 0.25, and 0.025 ps for the respective strain rates. This results in modest temperature fluctuations, which would lead to correct canonical averages of the system properties.[43] The system properties during each strain increment were computed by averaging over the final 2000 relaxation steps.

The localized axial stress state for atom i is defined as[44]

$$\eta_{zz}^i(\varepsilon) = \frac{1}{\Omega^i} \sum_{\substack{j=1 \\ (j\neq i)}}^{N} F_z^{ij}(\varepsilon) r_z^{ij}(\varepsilon), \tag{6}$$

where F_z^{ij} refers to the [001] vectoral component of the pairwise interatomic force between atoms i and j, obtained from Eq. (4). r_z^{ij} is the interatomic distance in the [001] direction between the ij pair. Ω^i refers to the volume of atom i, which was assumed as a hard sphere in a closely packed undeformed crystal structure. The axial stress on the nanowire is taken as the arithmetic mean of the local stresses on all atoms, as follows:

$$\sigma_{zz}(\varepsilon) = \frac{1}{N} \sum_{i=1}^{N} \eta_{zz}^i(\varepsilon). \tag{7}$$

From Eq. (7), the stress-strain response of the platinum nanowire could be obtained from the simulation statistics. The stress-strain response and Young's modulus of the nanowire could be analyzed and deduced.

III. SIMULATION RESULTS AND DATA ANALYSIS

The simulation results from the MD simulation will be presented here. Figures 2(a), 4(a), and 6(a) show the stress-strain relationship of the nanowire, simulated at 50 K, for strain rates of 0.04%, 0.4%, and 4.0% ps^{-1}, respectively. Figures 3(a), 5(a), and 7(a) show the corresponding results for the simulation at 300 K. Points where significant changes take place on the nanowire's crystal structure and stress-strain response were marked on the plot, indicated by numerical notations within angular brackets ⟨ ⟩. Its corresponding atomic arrangements were shown in Figs. 2(b)–7(b). Visualization of MD simulation was performed using the visual molecular dynamics (VMD) software, developed by the Theoretical Biophysics Group of the University of Urbana-Champaign (UIUC, USA).[45] The Young's modulus and Poisson ratio were obtained for the nanowire prior to the first yield strain only. The former was obtained from linear regression analysis of the scatter plot of the stress-strain response. The latter was similarly obtained on the scatter plot for the radial strain vs axial strain (ε_{rr}-ε_{zz}). The radial strain (ε_{rr}) is defined as $\varepsilon_{rr}=\Delta R/R_0$, where R is the radius of the nanowire at strain state ε_{zz}, R_0 is the radius of the nanowire at its initial state and $\Delta R=R-R_0$. R was obtained by considering the mean distance of the surface atoms from the centroidal axis of the nanowire, which would give an average radius at each strain state. A virtual experiment was conducted using eight different cutoff values for each temperature and strain rate. "Cutoff" refers to the radius around a reference atom i, beyond which the interatomic potential is truncated. This cutoff value will be used for the generation of the Verlet neighbor list.[46] Eight virtual test samples were simulated by varying the cutoff at approximately uniform intervals between 1.91a and 2.50a, where a is the equilib-

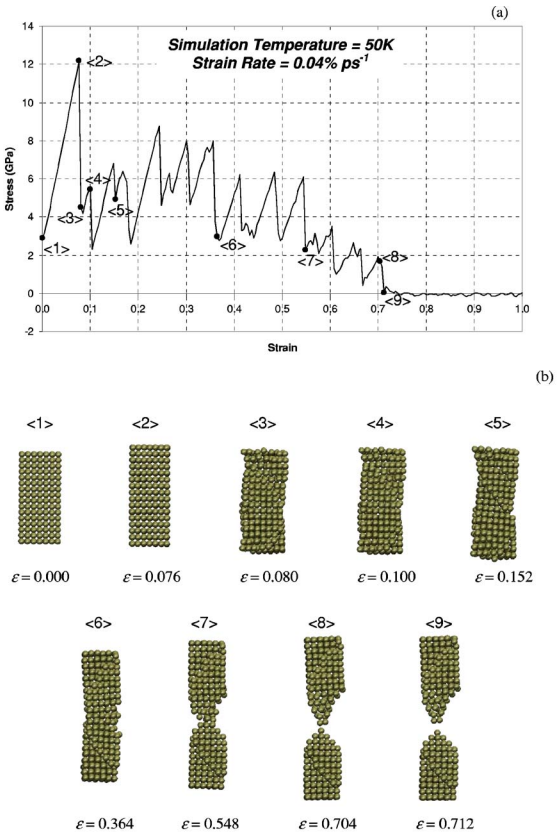

FIG. 2. (Color online) Stress-strain response of nanowire at $T = 50$ K and $\dot{\varepsilon} = 0.04\%$ ps^{-1}. (a) Stress-strain response with points where snapshots of the nanowire were captured and (b) snapshots of atomic arrangement of platinum nanowire at various strain values.

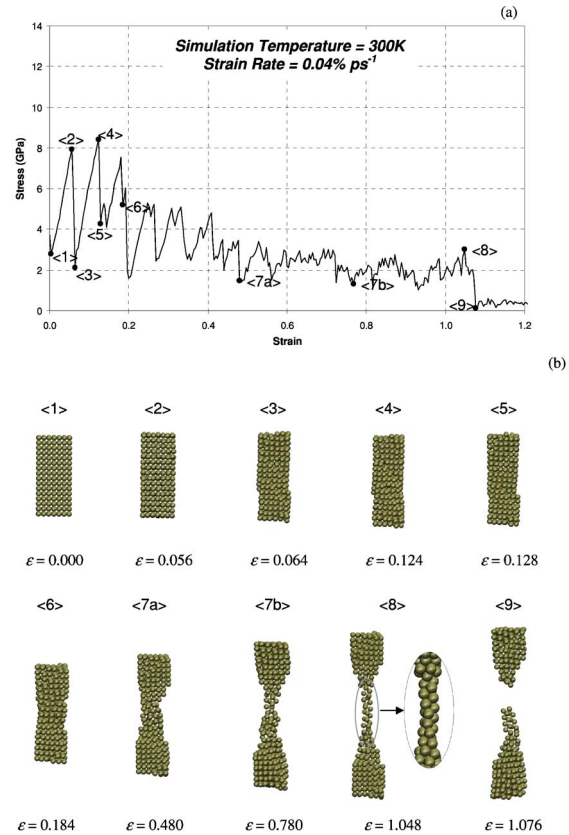

FIG. 3. (Color online) Stress-strain response of nanowire at $T = 300$ K and $\dot{\varepsilon} = 0.04\%$ ps^{-1}. (a) Stress-strain response with points where snapshots of the nanowire were captured and (b) snapshots of atomic arrangement of platinum nanowire at various strain values.

rium lattice parameter of platinum. The lower cutoff was adopted from Finbow *et al.*[27] In this case, the atomic interactions were truncated at 2.5 times the nearest neighbor distance a_{NN}, where $a_{NN} = a/\sqrt{2}$, with an additional $0.2a_{NN}$, imposed as the "skin." This was done in order to ensure stability and convergence of the algorithm. The upper cutoff represents the conventional value used for the Lennard-Jones pair potential,[33] with potential truncation at $2.5a_0$, where $a_0 \approx 0.9a$, and an additional $0.3a_0$ imposed as the "skin." Sample scatter plots for selected cutoffs at each simulated strain rate and temperature are shown in Figs. 8 and 9. Tables II and III show the values of the Young's modulus and Poisson ratio for all eight samples obtained from the virtual experiment. Table IV presents a summary for the mechanical properties of the platinum nanowire, as deduced from the MD simulation.

Figure 2 shows the stress-strain behavior of the nanowire, simulated at $T = 50$ K and $\dot{\varepsilon} = 0.04\%$ ps^{-1}, from its initial state to complete rupture. The extension of the nanowire commences with an elastic deformation from its initial state ⟨1⟩ to the first yield state ⟨2⟩. Upon reaching the first yield strain of $\varepsilon_{fy} = 0.076$, the crystal structure experienced an abrupt dislocation, as shown in Fig. 2(b) ⟨3⟩. Slippage occurred along the (111) plane and relaxed to a reconstructed configuration at ⟨3⟩. Such abrupt dislocation of fcc nanowires was previously reported by Todorov and Sutton[30] and Mehrez and Ciraci[31,32] for gold and copper nanowires, respectively, and result in quantum conductance jumps. As explained by Kang and Hwang[21] and Finbow *et al.*[27] the preferential occurrence of (111) slip planes is due to the smallest Burgers vector existing in the [110] close-packed directions for fcc crystal structures, making it most energetically favorable to reconstruct along this plane. After this, the nanowire recrystallized to a new, dislocated configuration and experienced a second dislocation after ⟨4⟩. It was observed that the strain and stress required to bring the nanowire from its most relaxed state after the initial slip to its second dislocation point was much smaller than that required to produce the first slip. This is because the reconstructed crystal structure has already relaxed to a minimum energy state after the initial slip, and any further deformation only involves an in-plane rearrangement of atoms, sliding along the (111) slip planes. Such a rearrangement process only requires a small amount of energy for the displacement of atoms. At ⟨5⟩, an out-of-plane slip was formed when the atoms around the middle section "climb" over other atoms, resulting in the development of an additional atomic layer. This reconstruction leads to a subsequent series of out-of-plane slips, which demand a 30% larger stress magnitude to achieve each successive dislocation and recrystallization between ⟨5⟩ and ⟨6⟩, compared to that between ⟨4⟩ and ⟨5⟩. During this process, the surface atoms were progressively displaced from their original locations, which subsequently results in surface rupture at ⟨6⟩. This significantly reduces the

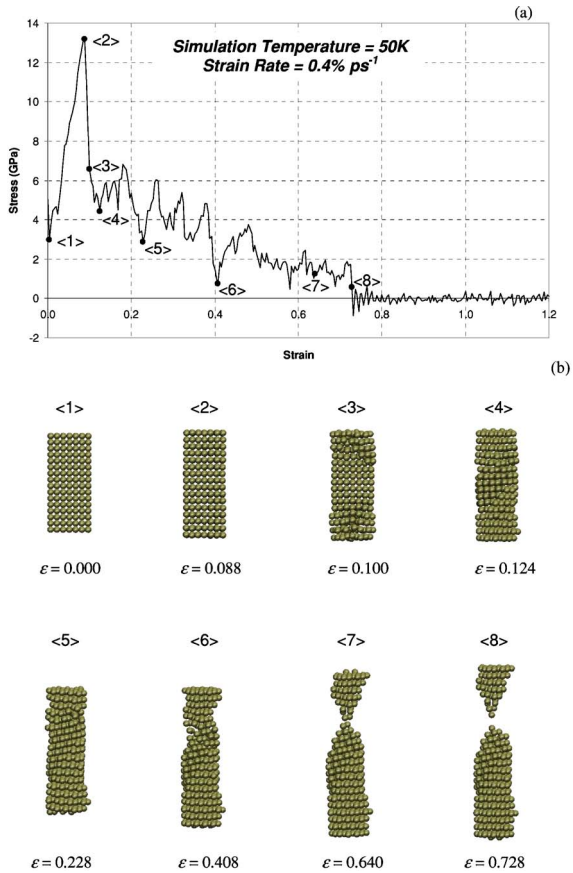

FIG. 4. (Color online) Stress-strain response of nanowire at $T=50$ K and $\dot{\varepsilon}=0.4\%$ ps^{-1}. (a) Stress-strain response with points where snapshots of the nanowire were captured and (b) snapshots of atomic arrangement of platinum nanowire at various strain values.

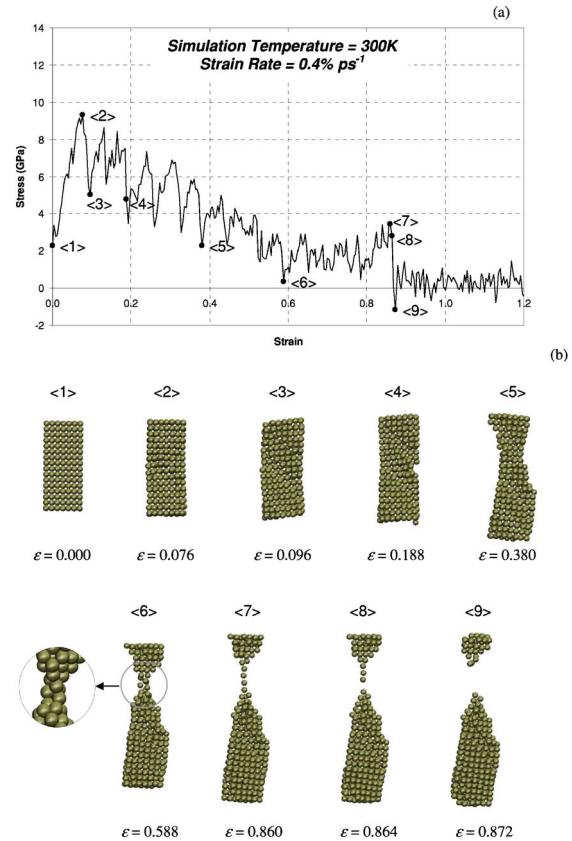

FIG. 5. (Color online) Stress-strain response of nanowire at $T=300$ K and $\dot{\varepsilon}=0.4\%$ ps^{-1}. (a) Stress-strain response with points where snapshots of the nanowire were captured and (b) snapshots of atomic arrangement of platinum nanowire at various strain values.

potential energy of the crystal structure and therefore the stress required to produce further dislocations was reduced by 25% after ⟨6⟩. During this process, necking of the nanowire commences. Significant necking occurs after ⟨7⟩ and complete rupture takes place at ⟨9⟩, with a rupture strain of $\varepsilon_{ru}=0.712$. This value was consistent with the results obtained by Finbow *et al.*[27] During the entire deformation process, it was observed that the nanowire reconstructs, relaxes, and recrystallizes in a stepwise, periodic manner, with clear peaks at the end of each recrystallization cycle. These well-defined periods of yielding are attributed to the tendency of the crystal structure to remain at its stable crystallographic configuration at this low temperature, where lattice order is highly preserved due to the relatively small atomic oscillations about their equilibrium positions.

At the higher temperature of $T=300$ K, the atomic structure has higher entropy, and its constituent atoms vibrate about their equilibrium positions at a much larger amplitude, as compared to that at $T=50$ K. It was observed from Fig. 3(a) ⟨2⟩ that the platinum nanowire has a 21% lower ε_{fy} and a corresponding 31% smaller σ_{fy}, as compared to Fig. 2(a). The onset of slip at $T=300$ K was expedited by the relative instability of the crystal structure due to a larger magnitude of oscillation about its equilibrium configuration, which disturbs the lattice order and encourages reconstruction of the crystal lattice. In-plane rearrangement and relaxation of atoms were also absent in this case, as the nanowire immediately reconstructed into a new configuration after the first yield cycle ⟨3⟩. Out-of-plane slippage occurred at a much lower strain of 0.064, and new atomic layers continued to form until $\varepsilon_{zz}=0.184$ ⟨4⟩, ⟨5⟩, and ⟨6⟩. After this, the surface atoms are dislodged ⟨6⟩ and necking begins. As a result of increased disorder of the crystal structure at $T=300$ K, the strain interval between onset of necking to overall rupture of the nanowire was increased. In the previous case [Fig. 2(a)], necking set in at $\varepsilon_{zz}=0.364$ and rupture occurred at $\varepsilon_{zz}=0.712$, giving an interval of $\Delta\varepsilon=0.348$ or $\Delta\varepsilon_D=34.8\%$, whereas, in this case [Fig. 3(a)], necking begins at a much smaller strain of 0.184, with rupture occurring at a 51% higher strain ⟨9⟩ of $\varepsilon_{ru}=1.076$, as compared to that at $T=50$ K. This gave $\Delta\varepsilon_D=89.2\%$ for $T=300$ K. The parameter $\Delta\varepsilon_D$ is defined as a measure of ductility of the nanowire. This means that the nanowire is about 55% more ductile at $T=300$ K than at $T=50$ K. A curious phenomenon could be observed here. At $\varepsilon_{zz}=0.780$, a double-helical structure begins to form at the narrowest part of the neck, which eventually developed to a clearly defined, single-layered helical structure at $\varepsilon_{zz}=1.048$ ⟨8⟩. It is interesting to note that the existence of a similar, single-walled helical platinum nanowire was reported by Oshima *et al.*[9] This 1.0 nm nanowire was synthesized by the electron-beam thinning method at a

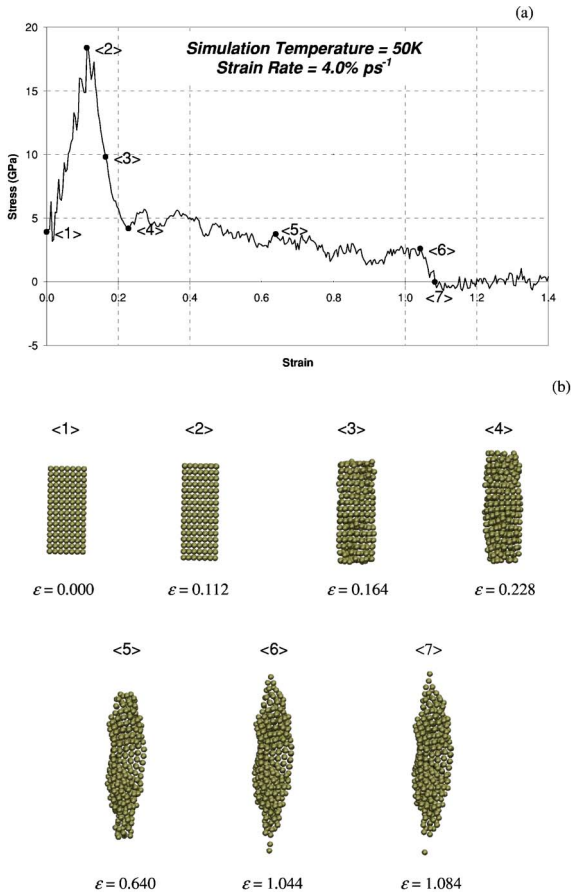

FIG. 6. (Color online) Stress-strain response of nanowire at $T=50$ K and $\dot{\varepsilon}=4.0\%$ ps^{-1}. (a) Stress-strain response with points where snapshots of the nanowire were captured and (b) snapshots of atomic arrangement of platinum nanowire at various strain values.

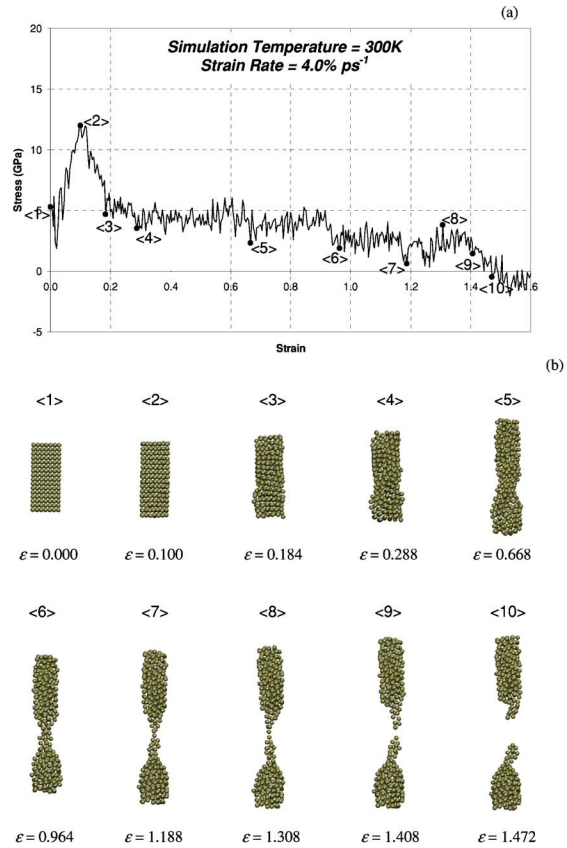

FIG. 7. (Color online) Stress-strain response of nanowire at $T=50$ K and $\dot{\varepsilon}=4.0\%$ ps^{-1}. (a) Stress-strain response with points where snapshots of the nanowire were captured and (b) snapshots of atomic arrangement of platinum nanowire at various strain values.

high temperature of 680 K. The resulting multishell nanowire was progressively thinned by electron migration through irradiation, until the innermost shell was exposed, producing the single-walled nanowire. In this MD simulation, the mechanical extension of a solid fcc nanowire at $T=300$ K revealed the same structure synthesized by Oshima *et al.* at $T=680$ K. Although it was not verified in this paper whether the helical structure, when it is isolated from the parent nanowire, will correspond to a stable atomic configuration, the emergence of this substructure contributed significantly to the overall ductility of the nanowire. This enabled the platinum nanowire to be strained beyond $\varepsilon_{zz}=1.000$, which displayed the important characteristic of superplasticity. Finally, a note could be put in place that a residual stress of about 3 GPa was observed after overall rupture of the nanowire. This probably indicates the presence of a stable substructure within the broken portions, which may be studied in detail in a separate investigation.

As $\dot{\varepsilon}$ was increased ten times from 0.04% to 0.4% ps^{-1}, the stress-strain response of the nanowire developed "minipeaks" or "wavelets" during the yielding cycles. This indicates the presence of disorder in the crystal lattice. The source of this disorder is attributed to the onset of amorphous deformation of the nanowire at a high strain rate. This phenomenon was reported by Ikeda *et al.*,[22] where continuous transformation to an amorphous metal from a perfect crystal was observed for Ni and NiCu nanowires, when they are subjected to strain rates of up to 5.0% ps^{-1}. This phenomenon was observed in Fig. 4(b), where deformation snapshots ⟨3⟩, ⟨5⟩, and ⟨6⟩ showed a less clearly defined slip plane, and atoms clustering into disordered arrays instead of reconstructing along the (111) plane, as was observed in Fig. 2(b), snapshots ⟨3⟩–⟨5⟩. But nevertheless, the strain rate of 0.4% ps^{-1} was still insufficient to cause complete transformation of the nanowire to an amorphous structure, as periodic yielding still showed up during the extension process in Fig. 4(a). As such, this strain rate corresponds to a transitional strain-rate value, from which the behavior of the platinum nanowire under tensile strain changes from an ordered, crystallographic deformation, to a disordered, amorphous deformation. The ε_{fy} and σ_{fy} of the nanowire at $T=50$ K was increased by 16% and 8%, respectively, as a consequence of the increased crystal disorder. The subsequent relaxation process after the first yield was less abrupt, occurring over a strain interval of 0.036, as compared to a near immediate relaxation to a reconstructed state for that at $\dot{\varepsilon}=0.04\%$ ps^{-1} [Fig. 2(a)]. The nanowire therefore exhibited a ductile slip behavior when the strain rate was increased. Nanowire necking set in at $\varepsilon_{zz}=0.228$, where the surface atoms were completely displaced and new layers were formed ⟨6⟩. Overall rupture occurred at $\varepsilon_{zz}=0.728$ ⟨8⟩, giving $\Delta\varepsilon_D=50.0\%$. There

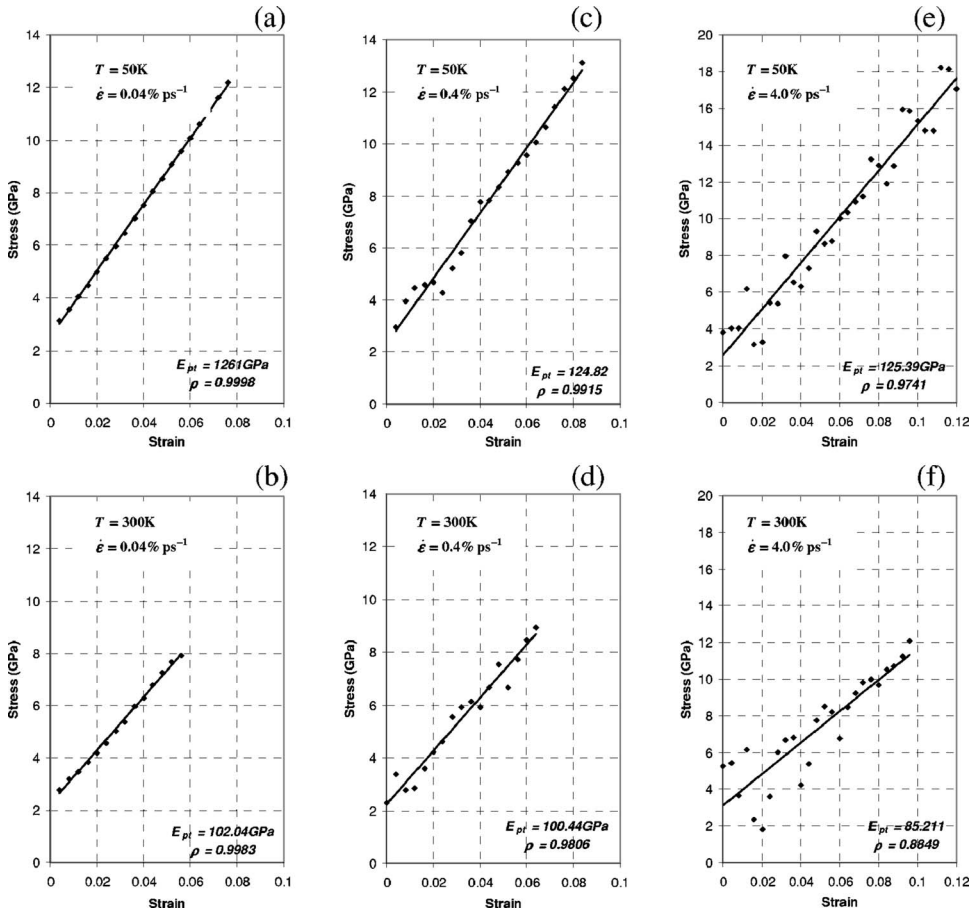

FIG. 8. Scatter plots for determination of Young's modulus.

was a 15.2% increase in overall ductility when the nanowire was deformed at $\dot{\varepsilon}=0.4\%$ ps^{-1} as compared to that at $\dot{\varepsilon}=0.04\%$ ps^{-1}, when the temperature was held constant at $T=50$ K.

Similar transitional amorphous behavior could also be observed at $T=300$ K. From Fig. 5(a), the first yield occurred at $\varepsilon_{fy}=0.076$ and $\sigma_{fy}=9.33$ GPa, which are 27% and 10% higher than the corresponding ε_{fy} and σ_{fy}, when the nanowire was subjected to a lower strain rate of 0.04% ps^{-1} [Fig. 3(a)]. (111) slip planes could be observed with relative clarity in this case in snapshots ⟨3⟩–⟨5⟩. Surface atoms begin to dislocate at $\varepsilon_{zz}=0.188$, and necking begins after ⟨4⟩. A single-walled helical structure, which was similar to that observed at $\dot{\varepsilon}=0.04\%$ ps^{-1}, had developed at the neck at $\varepsilon_{zz}=0.588$. But due to the higher strain rate, there was insufficient time for the structure to further relax and develop to a longer length. It was subsequently morphed into a single wire of platinum atoms ⟨7⟩ at $\varepsilon_{zz}=0.648$. The development length (L_d) of the single-walled helical structure for this strain rate was approximately $L_d=8.0$ Å, as compared to $L_d=20.0$ Å for $\dot{\varepsilon}=0.04\%$ ps^{-1}. This suggests that the single-walled structure developed in the nanowire, when it was subjected to $\dot{\varepsilon}=0.04\%$ ps^{-1}, is relatively more stable, with the longer developmental length contributing more significantly to the ductility of the parent wire, as compared to that at $\dot{\varepsilon}=0.4\%$ ps^{-1}. This also explains the peculiar observation of a larger overall ductility of the former ($\Delta\varepsilon_D=89.2\%$) compared to the latter ($\Delta\varepsilon_D=68.4\%$), which is contrary to the observations for $T=50$ K. Hence, the development of the single-walled helical substructure during axial deformation of the nanowire contributed very significantly to its superplasticity behavior, which more than offset the increase in ductility due to amorphous disorder of the crystal structure.

Finally, the nanowire was subjected to the highest strain rate of 4.0% ps^{-1}. In this simulation, the platinum nanowire exhibited superplasticity behavior right after yielding, and continued to deform up to rupture strains of $\varepsilon_{ru}=1.084$ and $\varepsilon_{ru}=1.472$ for that at $T=50$ and 300 K, respectively. The strain rate of 4.0% ps^{-1} had resulted in an amorphous rearrangement of the atoms positions for both simulations, as can be seen in snapshots ⟨3⟩ onward from Figs. 6(b) and 7(b). Due to a high degree of lattice disorder, the nanowire yielded at extremely high stresses of $\sigma_{fy}=18.35$ and 11.98 GPa, with corresponding strains of $\varepsilon_{fy}=0.112$ and 0.100 for $T=50$ and 300 K, respectively. This was up to 50% higher in σ_{fy} and 66% higher in ε_{fy} as compared to that simulated at $\dot{\varepsilon}=0.04\%$ ps^{-1}. The nanowire deformed uniformly, with no obvious necking until above $\varepsilon_{zz}=0.640$. This is an indication of superplastic behavior of metallic nanowires subjected to extremely high strain rates. The simulation at $T=50$ K showed necking occurring at the extreme ends of the nanowire [Fig. 6(b) ⟨5⟩–⟨7⟩]. This is probably a consequence of the MD simulation algorithm. Due to the application of a uniform strain along the [001] axis for every strain step, the atoms at the extreme ends of the simulation cell will be displaced first. The new positions of all other atoms away from the extreme ends will then be displaced progressively. Given sufficient relaxation time for all the atoms to relax into their

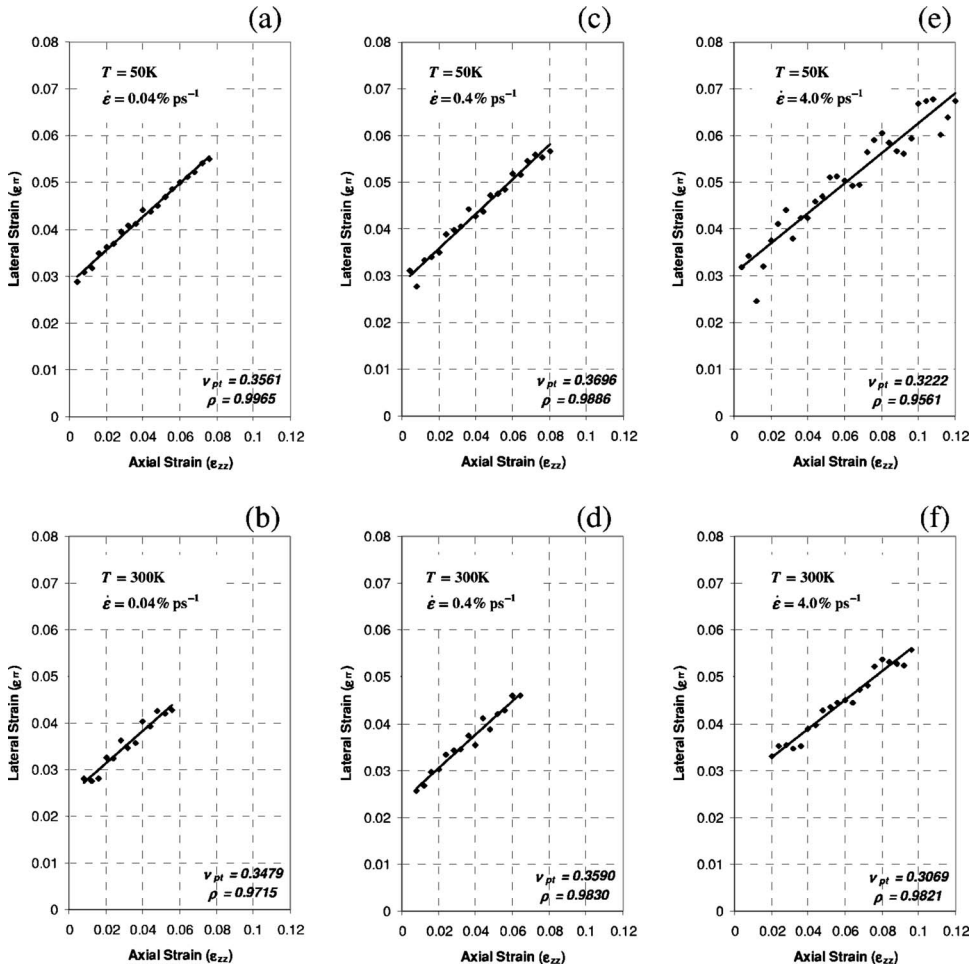

FIG. 9. Scatter plots for determination of Poisson ratio.

new positions, the nanowire will take up a new equilibrium configuration. In this case, due to the relatively low atomic velocities at $T=50$ K (since $\langle v^2\rangle=3kT/m$), the total relaxation time of 0.1 ps for each strain increment was apparently not sufficient for the nanowire to attain equilibrium. As such, at high strain magnitudes, atoms at the extreme ends were significantly displaced, while those around the middle region of the nanowire remained relatively undisturbed. Although equilibrium was not attained at each step, validity of the simulation results remained. That is because, given the accuracy of the empirical Sutten-Chen potentials in modeling mechanical properties of metallic systems,[37,38,41,42] including those subject to high strain rates,[22,23] this could be what is physically occurring in the platinum nanowire. In this situation, experimental verification must be performed to verify the simulations, which will require a separate investigation on its own. On the other hand, at $T=300$ K, due to the significantly larger ensemble average velocities of the system ($\langle v^2\rangle_{T=300\ \mathrm{K}}=6\langle v^2\rangle_{T=50\ \mathrm{K}}$), a much higher degree of equilibrium was attained at each strain step, as compared to $T=50$ K. As such, all atoms in the simulation cell were displaced and necking was observed within the nanowire [Fig.

TABLE II. Young's modulus (GPa) of platinum nanowire of eight virtual samples.

		$\dot{\varepsilon}=0.04\%$ ps^{-1}		$\dot{\varepsilon}=0.4\%$ ps^{-1}		$\dot{\varepsilon}=4.0\%$ ps^{-1}	
	Cutoff	50 K	300 K	50 K	300 K	50 K	300 K
Sample 1	1.91	125.52	101.92	124.82	103.85	125.13	84.94
Sample 2	1.95	125.60	99.79	125.53	108.83	125.39	85.21
Sample 3	2.00	126.26	102.04	126.08	96.24	125.87	85.50
Sample 4	2.10	125.81	100.66	125.61	100.44	125.72	85.21
Sample 5	2.20	126.02	101.97	125.11	95.88	125.45	84.93
Sample 6	2.30	125.22	100.90	125.17	92.35	125.49	85.04
Sample 7	2.40	126.23	98.13	125.28	99.66	125.66	85.15
Sample 8	2.50	126.10	100.25	125.18	103.24	125.59	85.10

TABLE III. Poisson ratio of platinum nanowire of eight virtual samples.

		$\dot{\varepsilon}=0.04\%$ ps^{-1}		$\dot{\varepsilon}=0.4\%$ ps^{-1}		$\dot{\varepsilon}=4.0\%$ ps^{-1}	
	Cutoff	50 K	300 K	50 K	300 K	50 K	300 K
Sample 1	1.91	0.3592	0.3754	0.3696	0.3601	0.3223	0.3068
Sample 2	1.95	0.3533	0.3682	0.3697	0.3981	0.3222	0.3067
Sample 3	2.00	0.3562	0.3479	0.3692	0.3668	0.3223	0.3065
Sample 4	2.10	0.3570	0.3869	0.3698	0.3590	0.3223	0.3069
Sample 5	2.20	0.3498	0.4095	0.3693	0.3970	0.3224	0.3068
Sample 6	2.30	0.3480	0.3661	0.3689	0.3962	0.3224	0.3067
Sample 7	2.40	0.3529	0.4048	0.3688	0.3989	0.3224	0.3068
Sample 8	2.50	0.3561	0.3785	0.3689	0.3953	0.3224	0.3068

7(b), ⟨7⟩–⟨10⟩]. It was further observed that there was no formation of a single-walled helical substructure, which meant that complete equilibrium was not attained at $T=300$ K. Instead, an amorphous lobe formed at the neck at $\varepsilon_{zz}=1.308$, which result in a slight increase in stress at ⟨8⟩ of Fig. 7(b). The nanowires rupture at $\varepsilon_{ru}=1.084$ and 1.472 for $T=50$ and 300 K, respectively, with corresponding ductility of $\Delta\varepsilon_D=85.6\%$ and 118.4%. In these cases, the platinum nanowires exhibited clear superplasticity behaviors.

A virtual experiment was conducted to determine the Young's modulus and Poisson ratio of the nanowire at the respective temperatures and strain rates. Only the results of one out of eight samples were presented here in Figs. 8 and 9. Figure 8 presents the scatter plots of the stress-strain response before the first yield state for all three strain-rate values, and Fig. 9 shows that of the ε_{rr}-ε_{zz} relationship. Linear regression analysis[47] was performed to produce a least squares, best-fit straight line through the sample points. The degree of linearity was quantified by the strength of correlation between the x and y coordinates of the sample points, known as the correlation coefficient (ρ). In a physical sense, it measures the stability of the crystal lattice when the nanowire undergoes axial deformation. As such, $\rho=100\%$ indicates a perfectly stable crystal lattice under deformation, where its constituent atoms do not oscillate about its equilibrium position (for example, at $T=0$ K). In this case there is perfect linearity in all its mechanical properties. On the other extreme, $\rho=0\%$ implies a completely random cluster of atoms under Brownian motion (for example, rare gases). In this simulation, ρ is larger than 88% at all strain rates, which indicates strong linearity in terms of stress-strain and ε_{rr}-ε_{zz} before first yield sets in. Analysis of eight samples showed that the Young's modulus was $E_{\mathrm{Pt}}=126$ GPa for the nanowire at $T=50$ K, with no significant difference observed for the different strain rates. On the other hand, it was $E_{\mathrm{Pt}}=100$ GPa at $T=300$ K for $\dot{\varepsilon}=0.04\%$ and 0.4% ps^{-1}, and dropped to $E_{\mathrm{Pt}}=85$ GPa for $\dot{\varepsilon}=4.0\%$ ps^{-1}. Firstly, it is noted that the Young's modulus obtained from the simulation was 50% to 75% that of its bulk Young's modulus ($E_{bulk}=168$ GPa). This was due to the nonexact fit between the calculated Young's modulus from the fitted potential and the experimental Young's modulus of the material. Sutton and Chen[38] showed that the experimental elastic constant (C_{11}) of platinum was about 15% larger than the computed modulus from the fitted potential. This was apparent from the analysis of the nanowire at 50 K, where correlation between the stress and strain points before first yield was very strong and thermal effects at the nanoscale were negligible. Second, it was noted that E_{Pt} was about 21% smaller at $T=300$ K. This was due to the significantly weakened bond forces due to the large atomic vibrations at the higher temperature, which resulted in a less stiff nanowire. Last, there was a 15% drop in E_{Pt} when the nanowire was subjected to the highest strain rate of 4.0% ps^{-1} at $T=300$ K. This is the result of a

TABLE IV. Summary of mechanical properties of platinum nanowire.

		$\dot{\varepsilon}=0.04\%$ ps^{-1}		$\dot{\varepsilon}=0.4\%$ ps^{-1}		$\dot{\varepsilon}=4.0\%$ ps^{-1}	
Property		50 K	300 K	50 K	300 K	50 K	300 K
First yield	ε_{fy}	0.076	0.060	0.088	0.076	0.112	0.100
	σ_{fy}[a]	12.19	8.47	13.18	9.33	18.35	11.98
Rupture	ε_{ru}	0.712	1.076	0.728	0.872	1.084	1.472
Ductility	$\Delta\varepsilon_D$	34.8%	89.2%	50.0%	68.4%	85.6%	118.4%
Young's modulus	E_{Pt}[a]	125.8	100.7	125.3	100.1	125.6	85.1
	ρ	99.98%	99.82%	99.10%	98.35%	97.39%	88.45%
Poisson ratio	ν_{Pt}	0.3541	0.3797	0.3693	0.3839	0.3223	0.3068
	ρ	99.73%	97.16%	98.85%	98.59%	95.59%	98.20%

[a]Units in GPa.

high degree of disorder introduced by the high strain rate and, coupled with the high temperature, amorphous melting of the crystal structure sets in. Finally, there was no significant difference in the Poisson ratio of the platinum nanowire as compared to the bulk value of 0.38, when it is subjected to the lower strain rates of 0.04% and 0.4% ps^{-1}. A 4%–6% lower value was observed for the nanowire at $T=50$ K, which simply means that the material is marginally more compressible at lower temperatures, due to a lower kinetic energy of the system. There was a further 11% and 20% reduction in Poisson ratio at $T=50$ and 300 K, respectively, when the nanowire undergoes amorphous deformation at $\dot{\varepsilon}=4.0\%$ ps^{-1}. This is due to higher malleability as a result of crystal lattice disorder. The development of short-ranged order of the crystal structure increases its ductility and, therefore, enhances its malleability and compressibility. This was marginally more evident at $T=300$ K as the material was undergoing amorphous melting at that temperature and strain rate. This resulted in a 5% smaller Poisson ratio than that at $T=50$ K.

IV. CONCLUSION

This paper presented the MD simulation of a platinum nanowire, subjected to axial deformation in the [001] direction. Several interesting features relating to its crystal structure and mechanical properties were observed when the nanowire was simulated under different strain rates at $T=50$ and 300 K. The crystal structure remained in its crystalline order at the lowest strain rate, with planar dislocation and slippage occurring along the (111) plane. Due to the higher crystal stability at $T=50$ K, the deformation behavior of the nanowire was characterized by brittle slips and brittle rupture, with very low ductility. At the higher temperature of 300 K, the crystal structure became less stable due to higher amplitude of vibration of the atoms about their atomic positions. A relatively stable single-walled helical substructure was formed due to the higher local vibration amplitude of the platinum atoms. This helical substructure enhances the ductility of the nanowire. The strain rate of 0.4% ps^{-1} was a transitional stage, where the deformation of the nanowire changes from a crystalline to an amorphous reconstruction. Some disorder was observed within the displaced mass of atoms, while the slip plane was still relatively well defined. The stress-strain relationship was also less strongly correlated during initial elastic deformation. The single-walled helical substructure was still observed at $T=300$ K, but did not have sufficient relaxation time to attain sufficient development length (L_d), giving less contribution to its overall ductility. The maximum strain rate of 4.0% ps^{-1} results in a completely amorphous deformation, where the nanowire displayed superplastic behavior. The first yield stresses and strains were more than double those simulated at $\dot{\varepsilon}=0.04\%$ ps^{-1}. Complete rupture was attained when it deformed up to more than twice its original length. Finally, it was found that the Young's modulus of the platinum nanowire was 50%–75% that of the Young's modulus of bulk platinum. The calculated Young's modulus of the nanowire at $T=300$ K was only about 50% that of bulk platinum, and was significantly smaller than that at $T=50$ K. This illustrated the atomistic size effect, giving material properties at the nanoscale that differed from its bulk properties. The Poisson ratio was not significantly different at the nanoscale as compared to the bulk, but was reduced up to 20% under high strain rate. The findings of this paper have laid the groundwork for further investigations into other mechanical behaviors of metallic nanowires like axial compression, shear, and twisting deformation. Future investigations could look into the stability and properties of the double-helical substructure, both experimentally and using computational simulation. The results could also serve as a guideline for subsequent experimental investigations, and the mechanical properties obtained could be used as input for linear continuum modeling of platinum nanostructures.

ACKNOWLEDGMENT

This work was funded by the Agency for Science, Research and Technology (A*STAR), Science and Engineering Research Council (SERC).

[1] J. L. Beeby, *Condensed Systems of Low Dimension*, NATO Advanced Study Institute, Series B: Physics (Plenum Press, New York, 1991), Vol. 253.
[2] S. Dubois, L. Piraux, J. M. George, K. Ounadjela, J. L. Duvail, and A. Fert, Phys. Rev. B **60**, 477 (1999).
[3] A. Christ, T. Zentgraf, J. Kuhl, S. G. Tikhodeev, N. A. Gippius, and H. Giessen, Phys. Rev. B **70**, 125113 (2004).
[4] N. Agraït, G. Rubion, and S. Vieira, Phys. Rev. Lett. **74**, 3995 (1995).
[5] H. Kido, Technical Report (Materials), Osaka Municipal Technical Research Institute, 2002 (unpublished).
[6] Y. H. Shao, M. V. Mirkin, G. Fish, S. Kokotov, D. Palanker, and A. Lewis, Anal. Chem. **69**, 1627 (1997).
[7] H. H. Byung, C. B. Sung, C. W. Lee, S. Jeong, and S. K. Kwang, Science **294**, 348 (2001).
[8] Z. L. Wang, R. P. Gao, Z. W. Pan, and Z. R. Dai, Adv. Eng. Mater. **3**, 657 (2001).
[9] Y. Oshima, H. Koizumi, K. Mouri, H. Hirayama, and K. Takayanagi, Phys. Rev. B **65**, 121401 (2002).
[10] L. B. Kong, M. Lu, M. K. Li, X. Y. Guo, and H. L. Li, Chin. Phys. Lett. **20**, 763 (2003).
[11] G. Rubio-Bollinger, S. R. Bahn, N. Agraït, K. W. Jacobsen, and S. Vieira, Phys. Rev. Lett. **87**, 026101 (2001).
[12] E. Tosatti, S. Prestipino, S. Kostimeier, A. Dal Corso, and F. D. Di Tolla, Science **291**, 288 (2001).
[13] B. L. Wang, S. Y. Yin, G. H. Wang, A. Buldum, and J. J. Zhao, Phys. Rev. Lett. **86**, 2046 (2001).
[14] F. Picaud, A. Dal Corso, and E. Tosatti, Surf. Sci. 532- **535**, 544 (2003).
[15] H. Y. Zhang, X. Gu, X. H. Zhang, X. Ye, and X. G. Gong, Phys.

Lett. A **331**, 332 (2004).
[16] F. Ercolessi, M. Parrinello, and E. Tosatti, Philos. Mag. A **58**, 213 (1988).
[17] M. S. Daw and M. I. Baskes, Phys. Rev. B **29**, 6443 (1984).
[18] S. P. Ju, J. S. Lin, and W. J. Lee, Nanotechnology **15**, 1221 (2004).
[19] G. J. Bilalbegovíc, J. Phys.: Condens. Matter **13**, 11531 (2001).
[20] A. V. Pokropivny, D. Erts, V. V. Pokropivny, A. Lohmus, R. Lohmus, and H. Olin, Phys. Low-Dimens. Semicond. Struct.1-**2**, 83 (2004).
[21] J. W. Kang and H. J. Hwang, J. Korean Phys. Soc. **38**, 695 (2001).
[22] H. Ikeda, Y. Qi, T. Çagin, C. Samwer, W. L. Johnson, and W. A. Goddard III, Phys. Rev. Lett. **82**, 2900 (1999).
[23] P. S. Branício and J. Rino, Phys. Rev. B **62**, 16950 (2000).
[24] R. H. M. Smit, Y. Noat, C. Untiedt, N. D. Lang, M. C. van Hemert, and J. M. van Ruitenbeek, Nature (London) **419**, 906 (2002).
[25] S. X. Lu and B. Panchapakesan, in *IEEE 2004 International Conference on MEMS, NANO and Smart Systems (ICMENS)* (IEEE Computer Society, Los Alamitos, CA, 2004), p. 36.
[26] A. Husain, J. Hone, H. W. C. Postma, X. M. H. Huang, T. Drake, M. Barbic, A. Scherer, and M. L. Roukes, Appl. Phys. Lett. **83**, 1240 (2003).
[27] G. M. Finbow, R. M. Lynden-Bell, and I. R. McDonald, Mol. Phys. **92**, 705 (1997).
[28] Q. H. Cheng, H. P. Lee, and C. Lu, Mol. Simul. **31**, 289 (2005).
[29] A. P. Sutton and J. B. Pethica, J. Phys.: Condens. Matter **2**, 5317 (1990).
[30] T. N. Todorov and A. P. Sutton, Phys. Rev. B **54**, R14234 (1996).
[31] H. Mehrez and S. Ciraci, Phys. Rev. B **56**, 12632 (1997).
[32] H. Mehrez, S. Ciraci, C. Y. Fong, and Ş. Erkoç, J. Phys.: Condens. Matter **9**, 10843 (1997).
[33] J. M. Haile, *Molecular Dynamics Simulation, Elementary Methods* (John Wiley & Sons, Singapore, 1992).
[34] F. Ercolessi, *A Molecular Dynamics Primer*, Spring College in Computational Physics (ICTP, Trieste, 1997).
[35] J. P. Hansen and I. R. McDonald, *Theory of Simple Liquids* (Academic Press, London, 1976).
[36] C. Kittel, *Introduction to Solid State Physics* (John Wiley & Sons, Singapore, 1996).
[37] F. Ercolessi, M. Parrinello, and E. Tosatti, Philos. Mag. A **58**, 213 (1988).
[38] A. Carlsson, in *Solid State Physics*, edited by H. Ehrenreich and D. Turnbull (Academic Press, London, 1990), Vol. 43, p. 1.
[39] M. W. Finnis and J. E. Sinclair, Philos. Mag. A **50**, 45 (1984).
[40] D. Tománek, A. A. Aligia, and C. A. Balseiro, Phys. Rev. B **32**, 5051 (1985).
[41] F. Cleri and V. Rosato, Phys. Rev. B **48**, 22 (1993).
[42] A. P. Sutton and J. Chen, Philos. Mag. Lett. **61**, 139 (1990).
[43] H. J. C. Berendsen, J. P. M. Postma, W. F. van Gunsteren, A. DiNola, and J. R. Haak, J. Chem. Phys. **81**, 3684 (1984).
[44] M. F. Horstemeyer, M. I. Baskes, and S. J. Plimpton, Acta Mater. **49**, 4363 (2001).
[45] E. Caddigan, J. Cohen, J. Gullingsrud, and J. Stone, *VMD User's Guide* (University of Illinois and Beckman Institute, Urbana, 2003).
[46] M. P. Allen and D. J. Tildesley, *Computer Simulation of Liquids* (Clarendon Press, Oxford, 1990).
[47] A. H. S. Ang and W. H. Tang, *Probability Concepts in Engineering Planning and Design* (Wiley, New York, 1984).